Dimensional Analysis of a Novel Low-Pressure Device for the Production of Size-Tunable Nanoemulsions

Ines Souilem, Christophe A. Serra, René Muller, Yves Holl, and Michel Bouquey
Institut Charles Sadron (ICS) – UPR 22 CNRS, F-67034 Strasbourg, France

Christophe A. Serra, René Muller, and Michel Bouquey
Université de Strasbourg (UdS), École Européenne de Chimie, Polymères et Matériaux (ECPM), F-67087 Strasbourg, France

Christophe Sutter
Institut de Chimie et Procédés pour l'Energie, l'Environnement et la Santé (ICPEES) – UMR 7515 CNRS, F-67087 Strasbourg, France

DOI 10.1002/aic.14690
Published online December 3, 2014 in Wiley Online Library (wileyonlinelibrary.com)

A novel low pressure device was used to generate nanoemulsions of methyl methacrylate. This device is based on a strong elongational flow known to be more efficient than the shear flow for dispersive mixing. The influence of process parameters (pressure drop number of cycles, number and size of holes) and composition parameters (monomer fraction, surfactant concentration, etc) on droplet size has shown that the average droplet size can be tailored in the range 30–200 nm by adjusting these parameters. The objective of the present paper is to find correlations that relate the obtained droplet size to the studied process and composition parameters. This model is based on a dimensional analysis using the Buckingham theorem in order to determine appropriate dimensionless numbers. This approach represents a first step for scaling up the device besides giving a set of parameters allowing to achieve a given droplet size. © 2014 American Institute of Chemical Engineers *AIChE J*, 61: 23–30, 2015
Keywords: nanoemulsion, elongational flow, dimensional analysis, droplet size, viscosity, process parameter, model, correlation

Introduction

Nanoemulsions can be defined as oil-in-water emulsions with mean droplet diameters ranging from 50 to 500 nm. The terms submicron emulsion and miniemulsion are often used as synonyms. They are considered as metastable systems contrary to microemulsions which are thermodynamically stable.[1] Once formed, they can be stable for few hours to several months depending on the formulation and the process parameters.

Nanoemulsions are used in a wide variety of fields among which cosmetic[2] and pharmacological applications.[3] Their use for biomedical applications is in constant development mainly for targeting agents or for drug delivery.[4]

To elaborate a nanoemulsion, four components are to be used: a continuous phase, a dispersed phase, a surfactant and a hydrophobic agent. These two last components are used in order to avoid coarsening phenomena likely to destabilize the nanoemulsion.[5] The nature of the surfactant has been shown to have an influence on the droplet size and stability.[6] It allows avoiding the coalescence occurring when two droplets collide and merge even if this phenomenon is not the major destabilizing factor for nanoemulsion due to the small droplet size. Ostwald ripening is considered as the major destabilizing phenomenon for nanoemulsions. It is defined as the growing of the largest droplets at the expense of the smallest ones. This occurs because the chemical potential of small droplets is higher than the chemical potential of larger ones, thus smaller droplets tend to give material to the largest ones through mass transfer across the continuous phase. This phenomenon can be avoided by adding a hydrophobic agent allowing building an osmotic pressure tending to balance the Laplace pressure.[7]

The most common apparatus used to generate nanoemulsions are ultrasound generators,[8] rotor-stator mixers,[9] high pressure homogenizers,[10] and static mixers.[11] Standard ultrasonification and rotor stator mixers can generate nanodroplets but are not convenient for scale-up to commercial volumes and remain suitable for laboratory scale not to mention their lack of an effective control in the droplet size not to mention their lack of an effective control in the droplet size. The high pressure homogenizer, although working under high pressure, remains the most apparatus used for industrial applications.

Alternatively, static mixers represent another method to generate nanoemulsions. Farzi et al.[11] have shown the

Additional Supporting Information may be found in the online version of this article.

Correspondence concerning this article should be addressed to C.A. Serra at ca.serra@unistra.fr.

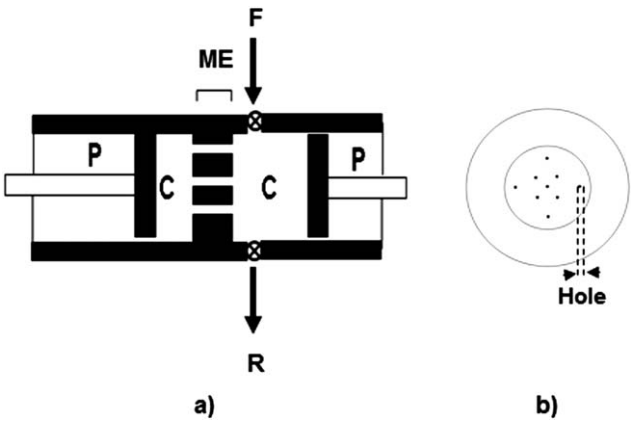

Figure 1. a) Schematic representation of the RMX® device: P pistons; C mixing chambers; ME mixing element; F: feeding channel; R: sampling and recovering channel. b) Front view of a typical mixing element, number of holes between 1 and 10, diameter of holes between 0.2 mm and 1 mm.

feasibility of nanoemulsions using such kind of mixer. Another generation of static mixers relying on the principle of elongational flow was recently designed.[12–15]

The influence of process parameters (such as the pressure drop ΔP between the chambers, the number of cycles, etc) and composition parameters (surfactant and hydrophobic agent concentrations, fraction volume of the dispersed phase, etc) was investigated and discussed in a first study.[12] Here, we complete our previous work by studying the influence of the geometry of the mixing element (number and size of holes, etc) and the viscosity ratio between the dispersed and continuous phase. Then, correlations between the obtained droplet sizes and process/composition parameters were extracted from experimental data using appropriate dimensionless numbers accounting for the process. These empirical correlations allow predicting the droplet size knowing experimental conditions or setting the process parameters to achieve a given size.

Experimental

Description of the emulsification device

The device used for emulsification, called RMX® (acronym stands for Reactor/MiXer), is schematically represented in Figure 1. Dispersed and continuous phases are alternately pushed, for a certain number of times, from one cylindrical chamber to the other through a central static mixing element characterized by a smaller section. This operation is carried at controlled pressure in the range 5–25 bars. One can estimate that the pressure applied on the upstream piston corresponds to the pressure drop ΔP between the chambers since the friction forces can be neglected.

The volume to be mixed depends on the position of the pistons and is easily adjusted in the range between 5 and 45 cm^3. Experiments of the present study were performed at room temperature and a thermocouple placed within the mixing element allowed to measure the temperature of the emulsion during time. One of the chambers is also fitted with a feeding channel for introducing all components into the device, and with an outlet channel to recover the final emulsion. The device is then operated on a multi pass basis, each cycle being composed of a back and forth displacement of the pistons and a prescribed number of cycles are chosen for a given experiment.

The static mixing element consists of a stainless steel plate with a given number of holes of adjustable diameter (Figure 1b). A first study describes in details the influence of all parameters for a mixing element of three holes having a diameter of 0.5 mm (the reference mixing element).[12] For the present article, different mixing elements were used to complete the study: the number of holes (n) was varied from 1 to 10 and the size of holes was varied between 0.2 and 1 mm.

Due to the contraction factor (CF) defined as the ratio between the cross-section of the chamber over the cross-section of holes, $\mathrm{CF} = \frac{d^2_{\mathrm{chamber}}}{n\, d^2_{\mathrm{hole}}}$, the material is submitted at each cycle to a convergent flow when pushed from the chamber into the holes and a divergent flow when moving from the holes into the downstream chamber. This convergent/divergent flow generates an elongational flow component known to be quite efficient for the mixing and droplet breakup.[16]

Materials

Emulsions are stabilized against coarsening through addition of a surfactant to prevent coalescence and a hydrophobic agent to slow down Ostwald ripening. Therefore, at least four components are required for the preparation of a nanoemulsion: oil, water, surfactant, and a hydrophobic agent. The oil phase was composed of methyl methacrylate (MMA, 99% purity, supplied by Aldrich, inhibited with 30 ppm of hydroquinone). The surfactant was sodium dodecyl sulfate (SDS, 99% purity, supplied by Alfa Aesar) and the hydrophobe was hexadecane (HD, 99% purity, supplied by Sigma Aldrich). Deionized water was used as the continuous phase.

Poly(methyl methacrylate) (PMMA) of a high molecular weight (120,000 g mol^{-1}) synthesized in the laboratory was used in order to increase the viscosity of the dispersed phase when necessary.

Emulsification procedure

The corresponding amounts of SDS and HD were respectively dissolved in deionized water and in MMA. Then, these two solutions were poured in a beaker and stirred under gentle agitation during 2 min with a magnetic stirrer before being introduced into the mixer. A certain number of cycles (Nc, typically Nc = 500) at a given pressure drop ΔP was then imposed. At the end of the emulsification step, the emulsion was recovered and characterized by dynamic light scattering (DLS). While using PMMA to increase the viscosity of the dispersed phase, the dry polymer was added to the oil phase along with HD, and then mixed with a stirring bar at room temperature until the polymer was completely dissolved. The solution was then added to the previously prepared surfactant solution. The viscosity of the system {MMA + HD + PMMA} was measured using an Ubbelhode viscometer of Category I. The interfacial tension measurements were carried on a tensiometer (Tracker model, TRK-S) from Teclis using the method of the rising drop. The droplet-size distribution was characterized by DLS using the Zetasizer Nano Series (Malvern) at a fixed scattering angle of 173°. DLS samples were prepared by diluting the original emulsion in a 100 times larger volume of deionized water immediately after recovering. The data given in the present study correspond to the volume average diameters D_v obtained after three different analyses performed on the same sample.

Table 1. Reference Values of Experimental Parameters

Water	85% vol
MMA	15% vol
[SDS]	4 g L^{-1}
[HD]	4% wt./MMA
ΔP	15 bars
Nc	500

Results and Discussion

The proposed RMX® nanoemulsification process can be described by two set of parameters: the process parameters consisting in the number of cycles (Nc), the pressure drop between the chambers (ΔP), the geometry of the mixing element (size, number, and length of holes); the physical parameters comprising the viscosity of the continuous (η_c) and dispersed (η_d) phases and the interfacial tension (σ), the last depending on the surfactant to monomer weight ratio. The influence of Nc, ΔP, and SDS concentration was already studied in details in a previous paper.[12] ΔP was varied from 5 to 20 and results have shown that D_v decreases from 100 nm down to a plateau value of 30 nm while increasing ΔP. It was found that D_v decreased when the SDS concentration was increased to reach a constant value for [SDS]/[MMA] $\cong$ 2.5%. The surface coverage was in the range of 20–60% indicating stable emulsions at least for few hours. A comparison between different emulsification devices, ultraturrax, ultrasonificator (US), high pressure homogenizer (HPH), and RMX®, was also performed. Results have shown that the sizes obtained with the RMX® are in the same range than those obtained with US and HPH for comparable mixing energies.

The previous study is now completed in this article by reporting the influence of the mixing element dimensionless parameters comprising the size (d_{hole}), the length (L_{hole}) and the number (n) of holes. The influence of the viscosity of the dispersed phase is also reported.

The reference values of all parameters are listed in Table 1. When studying the influence of a given parameter, all other parameters were kept to their reference value.

Influence of process and physical parameters

Influence of the Viscosity of the Dispersed Phase. The idea of increasing the viscosity ratio $p = \frac{\eta_d}{\eta_c}$ comes from Grace[17] who has shown that the shear flow is not convenient for droplet breakup when viscosity ratios are higher than four, and that the elongational flow is more convenient for such ratios. It was then interesting to study the feasibility of emulsions in the RMX® for p higher than one.

The viscosity of the continuous phase was kept constant and equal to 1 cP. The concentration of PMMA was varied between 1 and 10% on MMA weight base. The viscosity of the dispersed phase at these different concentrations was measured by means of an Ubbelhode viscosimeter (Categorie I). This method is based on the determination of the time necessary to the solution to flow through a capillary. Each measurement was repeated four times and a mean value for the flow time was taken. This time is then correlated to the kinematic viscosity (v) in cSt ($mm^2\ s^{-1}$) as follow

$$v = K(t - \theta) \tag{1}$$

where K is a constant related to the capillary (equal to 0.01 in our case), t is the average flow time (s) and θ is the Hagenbach correction of time (s). The dynamic viscosity (Pa s) is then

$$\eta = \rho v \tag{2}$$

As expected, p increases with the added amount of PMMA (Supporting Information Figure S1). For low concentrations of PMMA (<3%), the variation is quite linear and then follows a quadratic increase. A viscosity ratio of around five is reached with 10% of PMMA.

Emulsions were then performed in the RMX® and compared to the US and the ultraturrax. For the US, the experiment was done at 60% of the maximum power (450 W) and lasted for 15 min. For the ultraturrax, model KINEMATICA POLYTRON PT 10–35 GT having a maximum power of 800 W and generating shear flow, the experiment was made at 10,000 rpm for 15 min. Experiments with the RMX® were performed at the reference conditions of Table 1 using the reference mixing element ($n = 3$ and $d_{hole} = 0.5$ mm).

For the three devices, results are compared for a fixed mixing energy of 1500 J g^{-1} and illustrated in Figure 2.

It is shown that D_v increases almost linearly while p increases. As all other parameters were kept constant, the breaking of more viscous droplets with the same mixing energy leads to higher droplet size. Therefore, one should take into account the variation of the viscosity during the emulsification step for $p > 1$.

Influence of the Geometry of the Mixing Element. Based on the reference conditions, different geometries of the mixing elements were tested. The effects of the size, length, and number of holes are presented in the following.

Influence of the Length of the Hole. Due to geometry limitations of the drilling process, L_{hole} cannot exceed 4 mm. Four mixing elements differing only by the length of the hole (1, 2, 3, and 4 mm) were compared (Supporting Information Table S1). Experiments were performed for the reference composition of Table 1 and for $\Delta P = 15$ bars. No significant influence of L_{hole} in the range [1–4] mm was observed (Supporting Information Figure S2). This means that there is no influence of the regular pressure drop inside the hole. It would have been interesting to study mixing elements of L_{hole} higher than 4 mm which was not possible in our case due to geometric constraints in the drilling process used.

Influence of the Size of the Hole. Two different mixing elements were tested: the first corresponds to the reference one and the second is composed of three holes of diameter 0.8 mm, the CF being equal to 1365 and 533, respectively

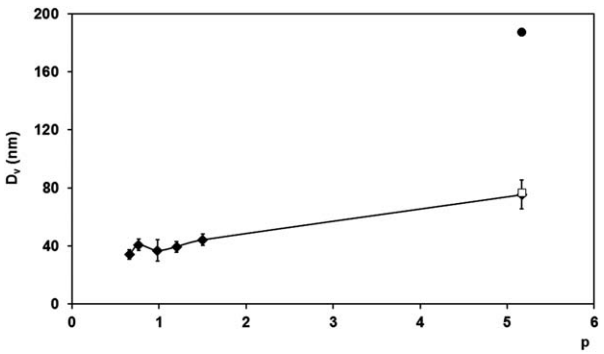

Figure 2. Influence of the viscosity ratio p on droplet size D_v: RMX® at ΔP = 15 bar (◆), Ultrasonification at 60% of amplitude (□) and Ultraturrax at 10000 rpm (●).

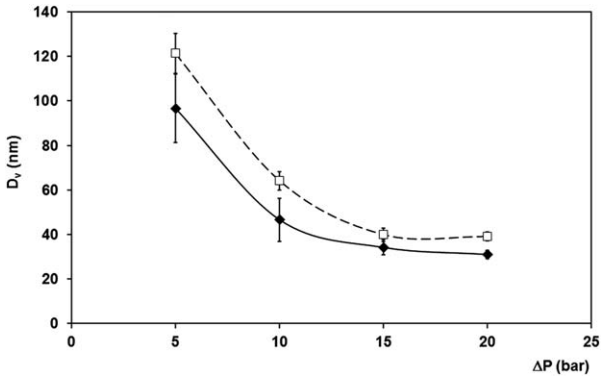

Figure 3. Influence of the hole diameter on droplet size for different mixing element size: ◆, solid line: ME 0.5 (3); □, dotted line: ME 0.8 (3).

(Supporting Information Table S2). The variations of the droplet size with respect to n for these two mixing elements are shown in Figure 3.

The evolution of D_v for both mixing elements follows the same trend: D_v decreases while increasing the pressure drop as reported earlier.[12] Droplets in the range 30–120 nm were generated with both mixing elements. However, droplet sizes generated with ME2 were slightly higher than with ME1. This can be explained by the fact that the elongational flow is more efficient when the CF increases: $CF_{ME1} \approx 3\,CF_{ME2}$.

An estimation of the elongational strain rate $\dot{\varepsilon}$ through the Cogswell's analysis[18] assuming that the emulsion is a Newtonian liquid is given by Eq. 3

$$\dot{\varepsilon} \cong \frac{\tau\,\dot{\gamma}}{\Delta P_{se}} \tag{3}$$

where τ is the shear stress, $\dot{\gamma}$ is the shear rate at the wall and ΔP_{se} is the entrance pressure drop near the abrupt contraction. Eq. 3 requires that ΔP_{se} has to be known. ΔP_{se} is given as follow[19]

$$\Delta P_{se} = \xi_e \frac{\rho_c <u>^2}{2} \tag{4}$$

where ξ_e is the fitting coefficient expressed as

$$\xi_s = \left[\frac{1}{0.59 + 0.41\left(\frac{d_{hole}}{d_{chamber}}\right)^3} - 1\right]^2 \tag{5}$$

$\dot{\gamma}$ is given as follow

$$\dot{\gamma} = \frac{4\,Q_{hole}}{\pi\,R_{hole}^3} \tag{6}$$

where Q_{hole} is the flow rate through a single hole and

$$\tau = \eta\,\dot{\gamma} \tag{7}$$

Results show that $\dot{\varepsilon}$ for ME 0.5 (3) is around three times more important than $\dot{\varepsilon}$ for ME 0.8 (3). This highlights the importance of elongational flow for high CFs.

Influence of the Number of Holes. Two mixing elements differing only by the number of holes (3 and 6) were compared (Supporting Information Table S3). Results show the same trend for both mixing elements (Supporting Information Figure S3). The conclusions given in the previous paragraph are also valid: D_v decreases and reaches a plateau value at 15 bars. The contraction factor $CF_{ME\ 0.5\ (3)}$ is twice as much as $CF_{ME\ 0.5\ (6)}$ meaning that for a fixed ΔP, the elongational flow component is more pronounced for more important CF, leading to smaller droplets.

Dimensional analysis

Different models exist in the literature to describe static mixers. These models correlate generally a mean diameter to the process and physical parameters by the use of dimensionless numbers. Most of them are derived from the approach of stirred tank.[20] These models can be divided into two categories: the first one is based only on the hydrodynamics[21] and are valid for low fractions of dispersed phase and the second ones are based on both hydrodynamics and physicochemistry of the system.[22–24]

These models are generally given as follow

$$\frac{d_{droplet}}{D} = C\,We^a\,Re^b\left(\frac{\eta_d}{\eta_c}\right)^c \tag{8}$$

where a, b, c, and C are constants depending on the geometry of the static mixer, D is the diameter of the empty tube, Re and We the Reynolds and Weber numbers, respectively.

Dimensionless Groups. Following the same approach, we tried to find correlations in between dimensionless numbers which account for our experimental data. Using the Buckingham theorem,[25] one can define 11 variables: $d_{droplet}$, $d_{chamber}$, d_{hole}, L_{hole}, n, ρ_d, ρ_c, η_d, η_c, v_{hole}, and σ. Where σ is the interfacial tension (N m^{-1}), $d_{chamber}$ is the size of the chamber, ρ_d and ρ_c represent, respectively the density of the dispersed and continuous phases (kg m^{-3}), η_d and η_c represent respectively the viscosity (Pa s) of the dispersed and continuous phases. As the values of the densities of the two phases are quite close and these two parameters have fixed values, we decided to consider a density ρ weighted relatively to ρ_d and ρ_c and given as

$$\rho = \varphi_v\,\rho_d + (1 - \varphi_v)\rho_c \tag{9}$$

where φ_v is the volume fraction of the dispersed phase.

This reduces the number of variables to 10. These variables are expressed in term of three independent fundamental physical quantities which are length (m), weight (kg), and time (s).

Then the original expression is equivalent to an equation involving a set of $10 - 3 = 7$ dimensionless parameters constructed from the original variables.

The first dimensionless number is $\frac{d_{droplet}}{d_{hole}}$. This number is the ratio of the droplet size over the hole size. The second one is the Reynolds number

$$Re = \frac{\rho\,v_{hole}d_{hole}}{\eta} \tag{10}$$

This number compares the inertial and the viscous forces, η corresponds to the emulsion viscosity which is a function of η_d and η_c. Different models are proposed in the literature.[26–29] Dukler et al.[28] proposed the following correlation which was used for our calculations

$$\eta = \varphi_v\,\eta_d + (1 - \varphi_v)\eta_c \tag{11}$$

The third number is the Weber number

$$We = \frac{\rho\,v_{hole}^2 d_{hole}}{\sigma} \tag{12}$$

which compares the inertial and interfacial forces. The ratio between the viscosities of the dispersed and continuous

phases is also a dimensionless number $p = \frac{\eta_d}{\eta_c}$. Only η_d varies in this study, η_c was kept constant. The last dimensionless numbers are related to the geometry of the mixing element and correspond to the number of holes n, the ratio $\frac{L_{hole}}{d_{hole}}$ and the ratio $\frac{d_{chamber}}{d_{hole}}$. The number of holes n has no physical meaning. It will be combined with the dimensionless number $\frac{d_{chamber}}{d_{hole}}$ to construct the CF defined as the ratio of the cross-section of the chamber over the whole cross-section of the holes.

$$CF = \frac{d_{chamber}^2}{n\, d_{hole}^2} \tag{13}$$

Based on the experimental data, one seeks an empirical relation describing $\frac{d_{droplet}}{d_{hole}}$ as a function of the other dimensionless numbers as follow:

$$\frac{d_{droplet}}{d_{hole}} = K\ \mathrm{Re}^{a}\,\mathrm{We}^{b}\,p^{c}\,\mathrm{CF}^{d}\left(\frac{L_{hole}}{d_{hole}}\right)^{e} \tag{14}$$

where K is a constant, a, b, c, d, and e are the exponents corresponding to the defined dimensionless numbers.

Elaboration of the Model. ***Description***. The method consists in using experimental data to determine each of the exponents a to e and is detailed in Supplementary Information. Roughly, it consists in selecting reference values for all the parameters included in the above mentioned dimensionless numbers (Supporting Information Table S4) and to make variation of one of them, keeping all other constant, so that only one dimensionless number will vary at the same time. On a logarithm plot giving the variation of $\frac{d_{droplet}}{d_{hole}}$ with respect to this specific dimensionless number, the slope of the curve will be equal to the exponent of that number.

Determination of the Exponents. Using Eqs. S4 and S5 and by plotting $\ln\left(\frac{d_{droplet}}{d_{hole}}\right)$ as a function of ln(Re), one founds the result of Figure 4 which gives $\beta = -1.68$. Equations S6 and S7 allow finding the value of $\alpha = 1.74$ (Figure 5).

The same procedure gives $c = 0.39$ and $e = -0.016$. The value of e is near 0, this means that there is no influence of the length of the hole as reported earlier (Supporting Information Figure S2). Finally, the model is given as follow

$$\frac{d_{droplet}}{d_{hole}} = K\,\mathrm{Re}^{1.79}\,\mathrm{We}^{-1.74}\,p^{0.39} \tag{15}$$

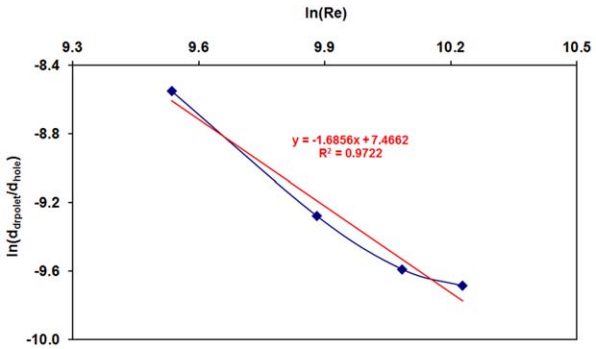

Figure 4. Determination of β.

[Color figure can be viewed in the online issue, which is available at wileyonlinelibrary.com.]

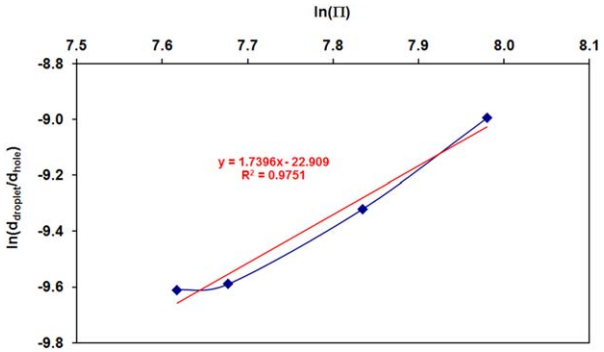

Figure 5. Determination of α.

[Color figure can be viewed in the online issue, which is available at wileyonlinelibrary.com.]

The value of the K constant is determined by taking into account all the experiments performed with the reference mixing element and calculating for each experiment a value of K using Eq. 15. The final mean value was found to be equal to 2.05×10^{-9}.

Thus, the model describing the reference mixing element ME 0.5 (3) is

$$\frac{d_{droplet}}{d_{hole}} = 2.05\times10^{-9}\,\mathrm{Re}^{1.79}\,\mathrm{We}^{-1.74}\,p^{0.38} \tag{16}$$

It was found that $a \approx -b$. This means that it is possible to combine Re and We into one dimensionless number which is $\mathrm{Ca} = \frac{\eta v_{hole}}{\sigma}$. This corresponds to the capillary number related to the hole which compares the influence of the viscous and interfacial forces.

The next step consists in optimizing the value of a, b, c, and K by taking into account all the experimental conditions investigated (see supplementary material). The values of the optimized parameters are given in Table 2. Note that these values differ somehow from those reported in Eq. 16 but account for all investigated conditions.

As seen in Figure 6, the new correlation (Eq. 16 with parameter values of Table 2) seems to reasonably describe the experimental data. The experimental points cluster around the diagonal. The lower and upper limits correspond to an error of 20% compared to the model. However, we note that the point in circle diverges from the model. The corresponding experiment was performed at a low pressure drop. The two other points on the same vertical correspond to the same experimental conditions. The difference between the three points is around 30 nm, while the difference between the duplicate points for other experimental conditions does not exceed 15 nm. Therefore we removed this point for further dimensional analysis as it most likely results from either experimental or analysis error.

Subsequently, the approach of linear regression was applied to the other mixing elements. Results have shown that the values of the exponents a and b are almost the same as those corresponding to the ME 0.5 (3).

Table 2. Values of the Optimized Parameters

Parameter	Value
A	1.39
B	−1.39
C	0.45
K	2.61×10^{-3}

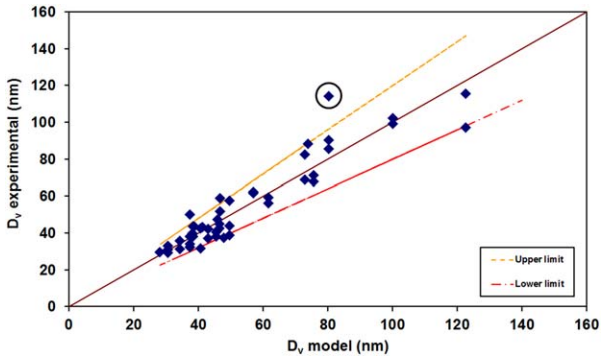

Figure 6. Comparison between the experimental droplet size and the model for the reference mixing element. Upper and lower limit correspond to ± 20% for the model prediction.

[Color figure can be viewed in the online issue, which is available at wileyonlinelibrary.com.]

Thus we kept the values of the optimized exponents a, b, and c given in Table 2 for all the mixing elements and tried to determine a value of K corresponding to each case (Supporting Information Table S5). It is possible to suppose that the constant K is a function of the CF

$$K = K' \, \mathrm{CF}^{\mathrm{d}} \tag{17}$$

$$\ln(K) = \ln\left(K'\right) + d \ln(\mathrm{CF}) \tag{18}$$

This approach allows providing an universal correlation valid for all the mixing elements. The variation of $\ln(K)$ depending on $\ln(\mathrm{CF})$ should follow a linear law of which d corresponds to the slope (Supporting Information Figure S4). Unfortunately, results do not show a linear variation of $\ln(K)$ as a function of $\ln(\mathrm{CF})$. This suggests that there are two or more correlations and that a single one cannot differentiate from the different mixing elements used. To validate this assumption, we chose to proceed on the basis of the general model given as follow

$$\frac{d_{\mathrm{droplet}}}{d_{\mathrm{hole}}} = K' \, \mathrm{Re}^{1.39} \, \mathrm{We}^{-1.39} \, p^{0.45} \, \mathrm{CF}^{d} \tag{19}$$

We considered all the experimental points obtained in the different experimental conditions and for the different mixing elements. Then, the droplet size is calculated through Eq. 19 by imposing arbitrary values of K' and d. Finally, we performed an optimization of K' and d according to the procedure described above. This optimization gives $K' = 8 \times 10^{-9}$ and $d = 1.75$. The model is then:

$$\frac{d_{\mathrm{droplet}}}{d_{\mathrm{hole}}} = 8 \times 10^{-9} \, \mathrm{Re}^{1.39} \, \mathrm{We}^{-1.39} \, p^{0.45} \, \mathrm{CF}^{1.75} \tag{20}$$

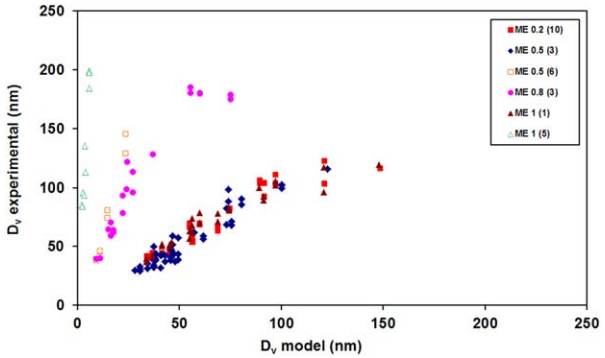

Figure 7. Comparison between the experimental data and the model for the 6 mixing elements tested.

[Color figure can be viewed in the online issue, which is available at wileyonlinelibrary.com.]

Figure 7 represents the experimental data as a function of the droplet size calculated through Eq. 20.

From Figure 7, one can clearly distinguish between the three different series (Supporting Information Table S6). The correlation given by Eq. 20 describes well the mixing elements of the series 1 as the points cluster around the diagonal. Based on this observation, it was possible to suggest that there is a dimensionless number among the considered numbers varying in different areas between the three series. Table 3 includes the minimum and maximum values for all the dimensionless numbers for the three series.

For Re, We, n, p, $\frac{d_{\mathrm{chamber}}}{d_{\mathrm{hole}}}$, and $\frac{L_{\mathrm{hole}}}{d_{\mathrm{hole}}}$, the minimum and maximum values for series 1, 2, and 3 overlap. This means that one cannot differentiate the series based on these numbers. The last line of Table 3 represents the values of the CF. One sees that each series has a range of CF independently of the other which seems to indicate that these three series can be distinguished based on their respective CF values.

We decided to eliminate series 3 from the dimensional analysis since it is described by a single mixing element and the few experimental points are not sufficient to give a reliable correlation. Finally, the model defined by Eq. 20 is valuable for series 1 as the points are arranged around the diagonal. It will be denoted Model 1.

The starting point to define the Model 2 describing the mixing elements of series 2 is the geometric dimensionless number CF as this last is the parameter differentiating the two series. This means that the exponents a, b, and c corresponding respectively to Re, We, and p keep their values of Model 1. Only the exponent d and the K constant are optimized.

After optimization, the two models are given as follow:

Model 1: $\mathrm{CF} > 1000 \quad \frac{d_{\mathrm{droplet}}}{d_{\mathrm{hole}}} = 8.06 \times 10^{-9} \, \mathrm{Re}^{1.39} \, \mathrm{We}^{-1.39} \, p^{0.45} \, \mathrm{CF}^{1.76}$

Model 2: $\mathrm{CF} < 1000 \quad \frac{d_{\mathrm{droplet}}}{d_{\mathrm{hole}}} = 1.45 \times 10^{-14} \, \mathrm{Re}^{1.39} \, \mathrm{We}^{-1.39} \, p^{0.45} \, \mathrm{CF}^{4.05}$

The limit of 1000 was chosen arbitrarily. It would be interesting to study mixing elements with $683 < \mathrm{CF} < 1024$ to check which model is valid in this range and to refine the limit. Figure 8 represents the superposition of the above two models (validation of each model is reported in Supporting Information Figures S5 and S6).

The upper and low limits correspond to a limit fixed at more or less 20% with respect to the models. Results show that the optimized models fit well with the experiment especially for sizes lower than 120 nm. Sizes higher than this value are generally obtained either at low v_{hole} or at low SDS concentration corresponding to relatively high values of interfacial tension σ. This leads to a bad control of size at these conditions and is reflected in Figure 6 by the points

Table 3. Minimum and Maximum Values for the Different Dimensionless Numbers

	Series 1		Series 2		Series 3	
Dimensionless number	Minimum value	Maximum value	Minimum value	Maximum value	Minimum value	Maximum value
Re	5500	55,000	12,000	44,200	27,600	48,000
We	262000	3×10^5	33600	3×10^5	2×10^5	7×10^5
p	0.66	5.17	0.66		0.66	
n	1	10	3	6	5	
$\frac{d_{chamber}}{d_{hole}}$	32	160	40	64	32	
$\frac{L_{hole}}{d_{hole}}$	4	5	3	4	5	
CF	1024	2560	533	683	205	

placed away from the first diagonal which is the case for example of the ME 0.8 (3) for sizes higher than 200 nm.

The domain of size between 120 and 160 nm is less dense. Indeed, the experimental conditions studied in our case are more favourable to generate sizes below 160 nm or even below 100 nm which was the aim of our study. However this does not exclude the possibility of generating larger sizes.

It is also noticed that the determined exponents are in a good agreement with the experiment. For example, the exponent of v_{hole} is equal to $a+2b=-1.39$ which means that D_v decreases while increasing v_{hole}. This was shown while studying the influence of ΔP. At the same time, the interfacial tension σ is raised to the power $-b=1.39$ meaning that D_v increases with σ. This was proved while studying the effect of the surfactant concentration. Indeed, when the SDS concentration decreases, σ increases and then larger droplets are generated.

Four experiments were performed with Styrene as the dispersed oil phase (less soluble than MMA) instead of the MMA and are also included in this dimensional analysis. These experiments were made with the ME 0.5 (3) and results correspond to Model 1. This shows that our model can be extended to other oil phases. However, these results are limited to only four experiments done at a fixed v_{hole}.

Results show that the same size can be generated in different ways; with different mixing elements and in different experimental conditions. For example a size of 80 nm can be obtained with different methods illustrated in Table 4. These correlations allow predicting the final droplet size for a given system and a given mixing element or to make an inventory of the different operating parameters allowing generating desired size.

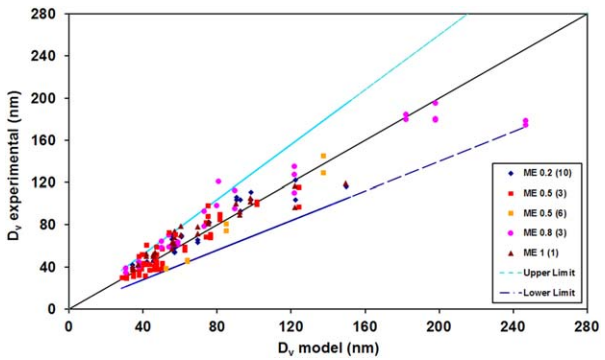

Figure 8. Superposition of models 1 and 2, upper and lower limit correspond to ± 20% for the model prediction.

[Color figure can be viewed in the online issue, which is available at wileyonlinelibrary.com.]

Conclusion

A new low pressure device (RMX®) primary designed for the elongational flow mixing of polymer blends[13] was used to produce nanoemulsions from low viscosity immiscible fluids. Completing a previous work aiming at investigating effects of some process (pressure, number of cycles) and composition parameters (amount of surfactant and Ostwald ripening inhibitor, volume fraction of the dispersed phase) on droplet size,[12] this study dealt with the influence of the mixing element geometry and viscosity ratio between continuous and dispersed phases. Although the length of the holes has little influence, their diameter and number significantly affect the size of the droplets formed. Moreover it was found that the device was still quite efficient to emulsify dispersed phases which viscosity is five times greater than that of the continuous phase, the droplet size increasing linearly with the viscosity ratio.

Furthermore, a dimensional analysis allowed finding a predictive model of the droplet size expressed as a set of two correlations. The difference between these correlations is made via the CF. The model takes into account the physical and process parameters and is comparable to those found in literature and describing static mixers.[20–24] It has the advantage to be more developed than those given in the literature because it takes into account the geometry of the mixing element. However, the model developed is not universal. It is only applied for the RMX® but can be extended to other oil phases than the two monomer phases investigated (methyl methacrylate and styrene).

This study should be completed in the future by studying the influence of the diameter of the chamber on the droplet

Table 4. Different Methods to Generate a Droplet Size of 80 nm

		Conditions				
		Mixing element				
Model	Method	n	d_{hole} (mm)	L_{hole} (mm)	V_{hole} (m s^{-1})	σ (mN m^{-1})
1	1	10	0.2	1	37	4.411
	2	3	0.5	2	26	3.768
	3	1	1	5	45	5.100
2	4	6	0.5	2	37	3.768

size. This parameter already exists in the dimensional analysis via the dimensionless number CF. However, variations of CF in this study were only due to the number (n) and diameter (d_{hole}) of the holes. This step would be necessary to scale up the RMX® to more important volumes and would require to build bigger RMXs®.

Acknowledgments

Authors acknowledge Christophe Melart and Thierry Djekrif for their contribution to the setup development.

Literature Cited

1. Salager JL, Antón R, Andérez, JM, Aubry J-M. Formulation des microémulsions par la méthode HLD, Techniques de l'ingénieur. Génie des Procédés. 2001; NJ2155:1–20.
2. Simonnet JT, Sonneville O, Legret S. Nanoemulsion based on phosphoric acid fatty acid esters and its uses in the cosmetics, dermatological, pharmaceutical, and/or ophthalmological fields, 2001, US Patent 6,274,150.
3. Harwansh RK, Patra KC, Pareta SK. Nanoemulsion as potential vehicles for transdermal delivery of pure phytopharmaceuticals and poorly soluble drug. *Int J Drug Deliv*. 2011;3(2):209–218.
4. Sarker DK. Engineering of nanoemulsions for drug delivery. *Curr Drug Deliv*. 2005;2(4):297–310.
5. Landfester K, Bechthold N, Tiarks F, Antonietti M. Formulation and stability mechanisms of polymerizable miniemulsions. *Macromolecules*. 1999;32(16):5222–5228.
6. Bouchemal K, Briançon S, Perrier E, Fessi H. Nano-emulsion formulation using spontaneous emulsification: solvent, oil and surfactant optimisation. *Int J Pharm*. 2004;280(1):241–25.
7. Landfester K. Recent developments in miniemulsions - formation and stability mechanisms. *Macromol. Symp*. 2000;150:171–178.
8. Landfester K, Eisenblätter J, Rothe R. Preparation of polymerizable miniemulsions by ultrasonication. *J Coatings Technol Res*. 2004;1(1):65–68.
9. Urban K, Wagner G, Schaffner D, Röglin D, Ulrich J. Rotor-stator and disc systems for emulsification processes. *Chem Eng Technol*. 2006;29(1):24–31.
10. Asua JM. Miniemulsion polymerization. *Progress Polym Sci*. 2002; 27(7):1283–1346.
11. Farzi G, Bourgeat-Lami, E, McKenna, TFL. Miniemulsions using static mixers: a feasibility study using simple in-line static mixers. *J Appl Polym Sci*. 2009;114(6):3875–388.
12. Souilem I, Muller R, Holl Y, Bouquey M, Serra CA, Vandamme T, Anton N. A novel low-pressure device for production of nanoemulsions. *Chem Eng Technol*. 2012;35(9):1692–1698.
13. Bouquey M, Loux C, Muller R, Bouchet G. Morphological study of two-phase polymer blends during compounding in a novel compounder on the basis of elongational flows. *J Appl Polym Sci*. 2011; 119(1):482–490.
14. Muller R, Bouquey M, Terrisse J. Dispositif mélangeur modulaire et instrumenté pour le mélange d'au moins deux matières visqueuses. 2008. Patent: WO02008142234.
15. Muller R, Bouquey M, Abbas L, Triki B. Un nouveau type de mélangeur: réalisation d'un prototype et premiers résultats. *Rhéologie*. 2007;12:27–36.
16. Khayat RE, Luciani A, Utrack LA, Godbille F, Picotd J. Influence of shear and elongation on drop deformation in convergent-divergent flows. *Int J Multiphase Flow*. 2000;26(1):17–44.
17. Grace HP. Dispersion phenomena in high viscosity immiscible fluid systems and application of static mixers as dispersion devices in such systems. *Chem Eng Commun*. 1982;14(3–6):225–277.
18. Cogswell FN. Converging flow of polymer melts in extrusion dies. *Polym Eng Sci*. 1972;12(1):64–73.
19. Darby R. Chemical Engineering Fluid Mechanics, 2nd ed. CNew Yor: Marcel Dekker, Inc., RC Press, 2001.
20. Canselier JP, Poux M. Procédés d'émulsification. Techniques et appareillage, Techniques de l'ingénieur. *Génie des Procédés*. 2004; 2(J2153):1–14.
21. Middleman S. Drop size distributions produced by turbulent pipe flow of immiscible fluids through a static mixer. *Ind Eng Chem Process Des Dev*. 1974;13(1):78–83.
22. Haas PA. Turbulent dispersion of aqueous drops in organic fluids. *AICHE J*. 1987;33(6):987–995.
23. Streiff F, Mathys P, Fischer T. New fundamentals of liquid-liquid dispersion using static mixers. *Récents Progrès en Génie des Procédés*. 1997;11(51):307–314.
24. Berkman PD, Calabrese RV. Dispersion of viscous liquids by turbulent flow in a static mixer. *AICHE J*. 1988;34(4):602–608.
25. Maa Y, Hsu C. Liquid liquid emulsification by static mixers for use in microencapsulation. *J Microencapsul*. 1996;13(4):419–433.
26. McAdams WH. *Heat Transmission*, 3rd Ed., New York: McGraw-Hill, 1954:83–85.
27. Cicchitti A, Lombardi C, Silvestri M, Soldaini R, Zavatarelli G. Two-Phase Cooling Experiments Pressure Drop, Heat Transfer and Burnout Experiments. *Energia Nucleare*. 1960;7(6):407–425.
28. Dukler AE, Wicks M, Cleveland RG. Frictional pressure drop in two-phase flow: A. A comparison of existing correlations for pressure loss and holdup / Frictional pressure drop in two-phase flow: B. An approach through similarity analysis. *AICHE J*. 1964;10(1):38–51.
29. Beattie D, Whalley P. A simple tow phase frictional pressure drop calculation method, *Int J Multiphase Flow*. 1982;8(1):83–87.

Manuscript received Mar. 20, 2014.